BIOCHEMISTRY
including biophysical chemistry & molecular biology

Article

pubs.acs.org/biochemistry

Decreased Amyloidogenicity Caused by Mutational Modulation of Surface Properties of the Immunoglobulin Light Chain BRE Variable Domain

Yuta Kobayashi,[†] Hirotaka Tsutsumi,[†] Tetsuyuki Abe,[†] Kyohei Ikeda,[†] Yuki Tashiro,[†] Satoru Unzai,[‡] Hironari Kamikubo,[§] Mikio Kataoka,[§] Hidekazu Hiroaki,[†,∥] and Daizo Hamada*[,†,⊥]

[†]Division of Structural Biology, Department of Biochemistry and Molecular Biology, Graduate School of Medicine, Kobe University, 7-5-1 Kusunoki-cho, Chuo-ku, Kobe 650-0017, Japan

[‡]Protein Design Laboratory, Yokohama City University, Suehiro 1-7-29, Yokohama 230-0045, Japan

[§]Laboratory of Bioenergetics and Biophysics, Nara Institute of Science and Technology (NAIST), Ikoma, Nara 640-0192, Japan

[∥]Laboratory of Structural and Molecular Pharmacology, Graduate School of Pharmaceutical Sciences, Nagoya University, Furo-cho, Chikusa-ku, Nagoya 464-8601, Japan

[⊥]Department of Life Sciences, Graduate School of Bioresources, Mie University, 1577 Kurimamachiya, Tsu, Mie 514-8507, Japan

Supporting Information

ABSTRACT: Amyloid formation by immunoglobulin light chain (LC) proteins is associated with amyloid light chain (AL) amyloidosis. Destabilization of the native state of the variable domain of the LC (V_L) is known to be one of the critical factors in promoting the formation of amyloid fibrils. However, determining the key residues involved in this destabilization remains challenging, because of the existence of a number of intrinsic sequence variations within V_L. In this study, we identified the key residues for destabilization of the native state of amyloidogenic V_L in the LC of BRE by analyzing the stability of chimeric mutants of BRE and REI V_L; the latter immunoglobulin is not associated with AL amyloidosis. The results suggest that the surface-exposed residues N45 and D50 are the key residues in the destabilization of the native state of BRE V_L. Point mutations at the corresponding residues in REI V_L (K45N, E50D, and K45N/E50D) destabilized the native state and increased amyloidogenicity. However, the reverse mutations in BRE V_L (N45K, D50E, and N45K/D50E) re-established the native state and decreased amyloidogenicity. Thus, analyses using chimeras and point mutants successfully elucidated the key residues involved in BRE V_L destabilization and increased amyloidogenic propensity. These results also suggest that the modulation of surface properties of wild-type V_L may improve their stability and prevent the formation of amyloid fibrils.

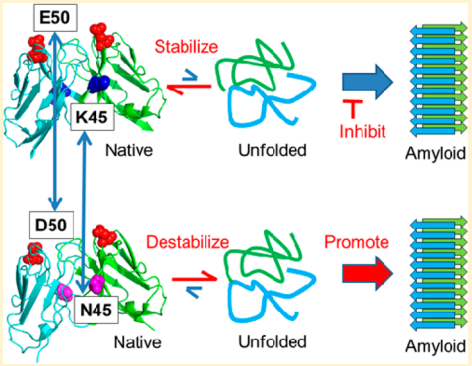

Proteins produced in their natural biological hosts generally fold into well-ordered native structures unique to their respective amino acid sequences, thereby achieving their unique functions.[1,2] However, proteins also tend to form insoluble aggregates both *in vivo* and *in vitro*, with varying condition-dependent morphologies.[3−7] Accumulation of fibrillar aggregates, namely amyloid fibrils, by proteins *in vivo* is often associated with various amyloid diseases. Nearly 30 different proteins are now known to be associated with amyloid diseases, including Alzheimer's disease, Parkinson's disease, type II diabetes, and amyloid light chain (AL) amyloidosis.[4,7−10]

Immunoglobulins play an important role in the biological defense against pathogens such as bacteria and viruses. These proteins consist of sets of heavy chains (HC) and light chains (LC), which comprise four and two immunoglobulin domains, respectively. Both HC and LC contain single variable domains (V_H and V_L, respectively), composed of complementarity-determining regions (CDR) containing hypervariable sequences, and framework regions (FR) containing relatively well-conserved amino acid sequences. The other domains in HC (C_{H1}, C_{H2}, and C_{H3}) and LC (C_L) comprise highly conserved amino acid sequences. The sequence variations in V_H and V_L, particularly within the CDR, allow individual immunoglobulins to interact with a wide variety of foreign molecules presented by different pathogens, thereby neutralizing their pathogenicity.

Normal plasma cells secrete not only properly folded, monoclonal immunoglobulins but also a small amount of free LC.[11] However, some malfunctioning plasma cells secrete mainly the free monoclonal LC, which results in various types of diseases such as multiple myeloma, light chain deposition disease (LCDD), and AL amyloidosis. AL amyloidosis is related

Received: June 25, 2014
Revised: July 18, 2014
Published: July 25, 2014

dx.doi.org/10.1021/bi5007892 | *Biochemistry* 2014, 53, 5162−5173

to the accumulation of amyloid fibrils formed by monoclonal LCs in various organs. In contrast, LCDD is associated with the accumulation of amorphous or granular aggregates of LC. Importantly, free LC is not always associated with such pathogenic aggregates *in vivo*. Epidemiological studies revealed that 10−15% of multiple myeloma patients also develop AL amyloidosis,[12−14] but most of these patients do not show any accumulation of amyloid fibrils formed by LC. Recent advances in chemotherapy targeting malfunctioning plasma cells, as well as in organ transplantation, have improved the clinical outcome of multiple myeloma patients.[15,16] These therapies also alleviate the symptoms of AL amyloidosis by eliminating the cells responsible for the production of the precursor proteins of amyloid fibrils.[15,17] However, the prognosis for AL amyloidosis patients remains suboptimal, possibly because damaged organs do not fully recover once they have been affected.[17]

Association of LCs into amyloid fibrils *in vivo* is most likely determined by the physicochemical properties conferred by the amino acid sequences of V_L. The destabilization of the LC native state is one of the most important factors determining the amyloidogenic propensity of V_L.[18−21] It is therefore of significant interest to develop a systematic strategy for identifying the key sequences involved in destabilization of the V_L, to understand the basic molecular mechanism underlying the pathogenicity of AL amyloidosis. Such information is also valuable in designing and producing antibodies used for therapeutics or for molecular and cell biology research. However, evaluating the relationship between sequence variation and amyloidogenicity is difficult and time-consuming because the number of possible sequence variations of V_L is too large to be tested.

To investigate this fundamental issue, in this study we analyzed the stability and amyloidogenic propensity of chimeric mutants between two highly homologous V_L forms of κ-type LC. One of these was from REI, an immunoglobulin LC originally isolated from a multiple myeloma patient who did not develop AL amyloidosis,[22] while the other was from BRE, an immunoglobulin LC originally isolated from an AL amyloidosis patient.[23,24] This approach successfully revealed two critical residues involved in the destabilization of the native state of BRE V_L, thereby promoting the formation of amyloid fibrils. Both of these residues are solvent-exposed in the native state. Furthermore, point mutations of these critical residues were observed to significantly increase the stability of the native protein and prevent the formation of amyloid fibrils.

MATERIALS AND METHODS

Preparation of Proteins. The cDNA of REI V_L was produced by combinations of PCR of short oligo DNAs with 40−70 bases using the KOD-Plus enzyme (Toyobo Co. Ltd., Osaka, Japan). The oligo DNAs were designed to have 12−22 bases of complementary sequences to another oligo DNA at 5′- and/or 3′-termini (see Table S1 of the Supporting Information). Artificially produced cDNA for BRE V_L was purchased from GenScript USA Inc. (Piscataway, NJ). All amino acid sequences were obtained from the NCBI database (http://www.ncbi.nlm.nih.gov), and the cDNA sequences were designed to enhance expression yields according to the codon usage of *Escherichia coli*. The produced cDNAs for REI and BRE V_L were introduced into pET28a (Novagen).

To produce the chimeric mutants, DNA fragments corresponding to the N-terminal region of REI V_L were amplified by PCR using plasmid DNA containing the wild-type REI V_L as the template. The resulting amplicons were employed as a set of megaprimers for the second round of PCR using plasmid DNA containing wild-type BRE V_L as the template. *E. coli* strain JM109 was transformed with these PCR products, and all transformants harboring plasmid DNA containing the chimeric mutant sequences were selected on LB plates supplemented with kanamycin.

The expression plasmids for the point mutant variants of REI and BRE V_L were prepared by inverse PCR using KOD-Plus as the PCR enzyme. *E. coli* BL21(DE3) cells harboring the corresponding plasmids were precultured in 10 mL of LB medium overnight at 37 °C and then transferred into 1 L of LB medium for further incubation at 37 °C. Protein expression was induced by addition of 1 mM IPTG when the OD_{600} of the cultures reached 0.6−0.7. The cultures were incubated for a further 4 h following induction, and the cells were then collected by centrifugation at 6000 rcf for 15 min. The collected cells were resuspended in 10 mL of 10 mM Tris-HCl (pH 8.0) containing 0.1 mM EDTA and 1.0 mg of hen lysozyme (Sigma-Aldrich), supplemented with 10 mg of deoxycholic acid that was added to the solution via manual mixing at 37 °C until the solution became viscous. Deoxyribonuclease I (1.0 mg; Sigma-Aldrich) was added to the suspension, and the mixture was further incubated at 37 °C until the viscosity of the solution decreased. The solution was then sonicated for further homogenization. Inclusion bodies were collected from the solution by centrifugation at 30000 rcf for 15 min. The collected inclusion bodies were rinsed twice with 10 mM Tris-HCl (pH 8.0) and dissolved in 10 mL of 10 mM Tris-HCl (pH 8.0) containing 8.0 M urea. The solubilized protein solution was incubated in a cold room at 4 °C while being shaken for 2 days to generate intramolecular disulfide bonds between C23 and C88 by air oxidation. The proteins were then refolded by dropwise dilution into 1.0 L of 10 mM Tris-HCl (pH 8.0) containing 0.1 mM EDTA. The solution was cleared by centrifugation at 6000 rcf and applied to a Q-Sepharose column (GE Healthcare) equilibrated with the same buffer. For REI V_L and its point mutants K45N, E50D, and K45N/E50D, the proteins were collected as a flow-through fraction, while the other V_Ls were eluted with a linear gradient from 0.0 to 1.0 M NaCl in 20 mM Tris-HCl (pH 8.0) containing 0.1 mM EDTA. The fractions containing the V_Ls were pooled and further purified by Superdex 75 size exclusion chromatography (GE Healthcare) and eluted with 10 mM Tris-HCl (pH 8.0) containing 0.1 mM EDTA.

Thermal Unfolding Monitored by Circular Dichroism (CD). Thermal unfolding experiments were performed using essentially the same method described by Hamaguchi et al.[25] CD spectra were obtained with a Jasco J-720W spectropolarimeter equipped with a Peltier-type thermo-controllable cell holder. A quartz cuvette with a path length of 1 cm was used. All data were expressed in terms of mean residue ellipticity, $[\theta]$ (degrees square centimeter per decimole). $[\theta]$ is defined as $100\theta_{obs}/(cl)$, where θ_{obs} is the observed ellipticity in degrees and c and l are the mean residue concentration of the protein (molar) and the path length of the cuvette (centimeters). The thermal unfolding reaction was monitored by measuring the ellipticity at 225 nm with a heating rate of 1 K min^{-1}. The resulting curves were analyzed by nonlinear least-squares curve fitting assuming the two-state mechanism of unfolding from the native to the unfolded state according to the Gibbs−Helmholtz equation, which is expressed as $\Delta G = (1 - T/T_m)\Delta H_m + \Delta C_p(T - T_m) + T\Delta C_p \ln(T_m/T)$, where ΔG and ΔC_p are the

dx.doi.org/10.1021/bi5007892 | *Biochemistry* 2014, 53, 5162−5173

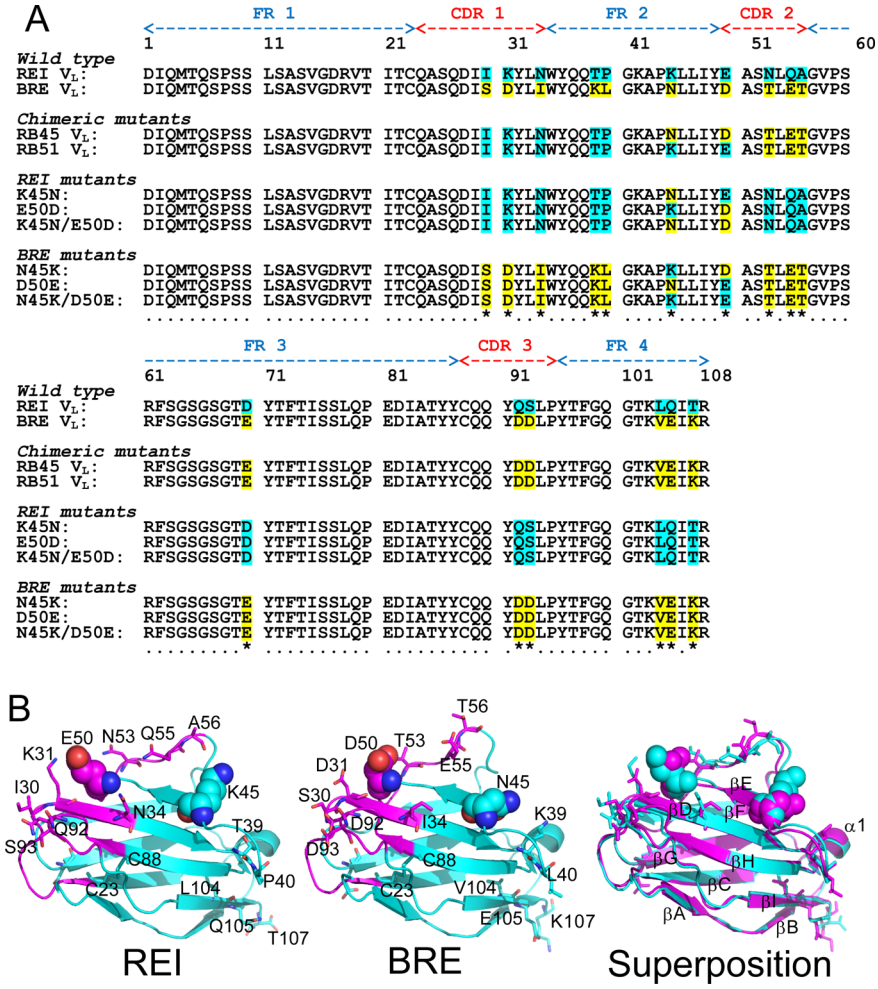

Figure 1. V_L variants prepared in this study. (A) Sequence alignments of wild-type REI and BRE V_L with their chimeric and site-specific point mutants. The amino acids highlighted in cyan and yellow are the residues commonly observed at these nonconserved amino acid positions in REI and BRE, respectively. Site-specific mutants of REI were designated as K45N, E50D, and K45N/E50D, while the BRE mutants were designated as N45K, D50E, and N45K/D50E. The regions corresponding with FR 1−4 and CDR 1−3 are indicated above the alignment. (B) Native structures of REI V_L (PDB entry 1REI) and BRE V_L (PDB entry 1BRE) as determined by X-ray crystallography. FR and CDR are colored cyan and magenta, respectively. The amino acids varying between REI and BRE V_L are represented with either space-filling models (residues 45 and 50) or stick models (the remainder). The conserved disulfide bond between C23 and C88 is also represented by a stick model. The structural superimposition of REI (cyan) and BRE (magenta) was calculated on the basis of the coordinates of the C_α atoms. The positions of the secondary structures (βA−βI and α1) are also indicated. The structural models were generated by PyMOL version 0.99 (http://www.pymol.org).

free energy and heat capacity changes upon unfolding at a given temperature, respectively, T is in kelvin, and T_m is the midpoint temperature of the unfolding reaction where $\Delta G = 0$. ΔH_m is the enthalpy change of unfolding at the T_m. ΔG is defined as $-RT \ln K_U$, where R is the gas constant and K_U is the equilibrium constant for the unfolding reaction at a given temperature, T. According to these equations, the fraction comprising the unfolded state (f_U) can be defined as $K_U/(1 + K_U) = [\exp(-\Delta G/RT)]/[1 + \exp(-\Delta G/RT)]$.

Thus, the theoretical curve for the unfolding reaction monitored by the ellipticity at 225 nm, $[\theta]_{225}$, can be expressed as $[\theta]_{N,225}(1 - f_U) + [\theta]_{U,225}f_U$, where $[\theta]_{N,225}$ and $[\theta]_{U,225}$ are the ellipticities at 225 nm for the native and unfolded states, respectively, at a given temperature. In practice, $[\theta]_{N,225}$ and $[\theta]_{U,225}$ are assumed to be linear functions of temperature. Curve fitting was performed with IgorPro 5.0 (Wavemetrics Inc., Lake Oswego, OR). All raw data were simultaneously fit to the equation described above assuming the following: $\Delta H_m = \Delta H_{ref} + \Delta C_p(T_m - T_{ref})$, where T_{ref} is the reference temperature and ΔH_{ref} is the enthalpy change upon unfolding of the protein at T_{ref}. T_{ref} was set to 310.15 K (37 °C) for all curve fitting analyses.

Fluorescence Spectroscopy. Fluorescence spectra were monitored with a FP-6500 fluorimeter (Jasco). For the detection of thioflavin T fluorescence, an excitation wavelength of 445 nm was used with monitoring emission wavelengths of 450−500 nm. To obtain the time course of amyloid formation, a 0.8 mg mL^{-1} protein solution in 10 mM sodium phosphate (pH 7.0) containing 150 mM NaCl was incubated at the given temperatures with rotation at 19 rpm using an RT-50 rotator (TAITEC, Saitama, Japan). Sample tubes were tightly sealed with parafilm to minimize the effects of evaporation of the water solvent during incubation. Aliquots of the sample solution were mixed with 10 volumes of a 5.0 μM thioflavin T solution in 10 mM sodium phosphate (pH 7.0) just prior to the fluorescence measurements.

The rates of amyloid formation were estimated from curve fitting analysis of the time-dependent change in thioflavin T

dx.doi.org/10.1021/bi5007892 | Biochemistry 2014, 53, 5162−5173

fluorescence based on the following stretched exponential function: $F = F_{final} + A \exp[-(k_{agg}t)^{\gamma}]$, where F is the observed fluorescence intensity, t is the time of incubation, and F_{final} is the final value of fluorescence intensity at infinite time. k_{agg} and γ are the rate constant and heterogeneity parameter, respectively.[26]

RESULTS

Design of Chimeric Mutants. Figure 1A indicates the sequence alignments between REI and BRE V_Ls as well as the chimeric and point mutant variants prepared in this study. Both REI and BRE belong to κ-type LC, and the level of sequence homology between REI and BRE V_L is 85%. Nine residues in the CDR (I30, K31, N34, E50, N53, Q55, A56, Q92, and S93 for REI and S30, D31, I34, D50, T53, E55, T56, D92, and D93 for BRE) differ between REI and BRE (Figure 1A). Six residues in the FR also differ between REI and BRE V_L [T39, P40, K45, L104, Q105, and T107 for REI and K39, L40, N45, V104, E105, and K107 for BRE (Figure 1)]. Both proteins contain a single disulfide bond between C23 and C88 (Figure 1B).

To roughly estimate the key residues associated with amyloid formation by BRE V_L, we initially designed two chimeric mutant combinations of REI and BRE V_L (RB45 and RB51, respectively), in which almost the entire C-terminal half of REI V_L is exchanged with that of BRE (Figure 1A). The RB45 mutant comprises the D1−P44 sequence from REI V_L, C-terminally fused to the N45−R108 sequence from BRE V_L. RB51 comprises the D1−E50 sequence of REI V_L fused to the A51−R108 sequence of BRE V_L. Thus, the K45N/E50D double mutant of RB45 V_L produces RB51 V_L.

The native structures of REI[27] and BRE V_L[23,24] were previously determined by X-ray crystallography, and both proteins are known to consist of nine β-strands, including βA (residues 4−7), βB (residues 10−13), βC (residues 19−25), βD (residues 31−38), βE (residues 45−48), βF (residues 62−67 for REI and residues 62−65 for BRE), βG (residues 70−75), βH (residues 84−90), and βI (residues 102−106), as well as one α-helix, α1, between βG and βH [residues 79−83 (see Figure 1B)]. The structures of these two proteins are highly superimposable with a root-mean-square deviation of only 0.56 Å based on the positions of the C_α atoms (Figure 1B). Thus, we expected that the chimeric mutants would assume conformations similar to the native structures of REI and BRE V_L under near-physiological conditions.

Amyloid Formation by Chimeric Mutants under Near-Physiological Conditions. To clarify the differences in amyloidogenic propensity between the chimeric mutants mentioned above and wild-type REI and BRE V_L, we analyzed the kinetics of amyloid fibril formation by these proteins on the basis of thioflavin T fluorescence (Figure 2A). The fluorescence intensity of thioflavin T increases around 490 nm when it is bound to amyloid fibrils. This unique property is very useful in estimating the amount of polypeptide molecules incorporated into amyloid fibrils[28,29] and for the direct observation of the rates of extension of single amyloid fibrils in combination with total internal reflection fluorescence microscopy.[30,31]

When the solutions containing 0.8 mg mL^{-1} V_L were incubated at pH 7.0 and 37 °C, only solutions containing either RB45 or BRE V_L showed an increased fluorescence intensity (Figure 2A). The time traces for aggregation as monitored by thioflavin T fluorescence produced sigmoidal curves showing clear lag phases, which are typical for nucleation-dependent reactions such as amyloid fibril formation. Thus, these results

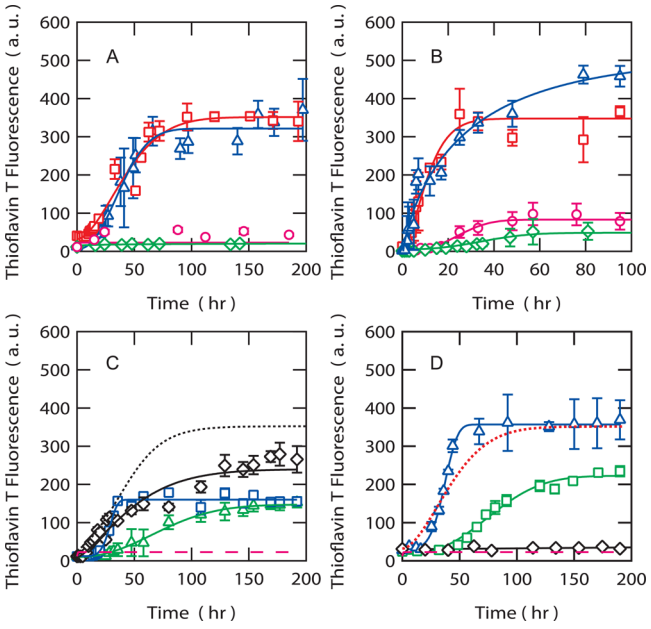

Figure 2. Kinetics of amyloid formation by V_L domains as monitored by fluorescence intensity upon thioflavin T binding. (A and B) Time traces of fluorescence intensities observed for REI (○), BRE (□), RB45 (△), and RB51 (◇) V_Ls at 37 (A) and 60 °C (B). (C) Time traces of fluorescence intensities observed for K45N (□), E50D (△), and K45N/E50D (◇) REI V_L at 37 °C. (D) Time traces of fluorescence intensities observed for N45K (□), D50E (△), and N45K/D50E (◇) BRE V_L at 37 °C. For comparison, the fitting results for wild-type REI and BRE V_L shown in panels A and B, respectively, are plotted as dashed and dotted lines in panels C and D. The reported kinetic traces were obtained by averaging results from three individual experiments. The error bars represent the standard error of the mean.

suggest that BRE and RB45 V_L were induced to form amyloid fibrils by incubation at 37 °C and pH 7.0 for prolonged periods of time. In contrast, solutions containing RB51 or REI V_L did not show any increase in thioflavin T fluorescence, suggesting that these proteins are unable to form amyloid fibrils, at least under the conditions employed here. These results also clarified that a difference at only two residue positions between RB45 and RB51 V_L can dramatically change the amyloidogenic propensity of the V_L domains.

Interestingly, when the proteins were incubated at 60 °C and pH 7.0, increased thioflavin T fluorescence was observed for all variants (Figure 2B). This result indicates that all the V_Ls studied here possess the intrinsic ability to form amyloid fibrils upon being incubated under conditions favoring the formation of unfolded states. However, the overall rates of amyloid formation are still dependent on the proteins involved, even at high temperatures. Thus, both BRE and RB45 V_L exhibited rates of amyloid formation much faster than those of REI and RB51 V_L, and the final amount of fibrils as estimated from thioflavin T fluorescence for the former set of proteins was also much larger than that for the latter. These differences in the rate and final intensity of thioflavin T fluorescence may be due to differences in thermodynamic stabilities among the V_Ls.

Equilibrium Thermal Unfolding by the V_Ls. It has been shown that destabilization of the native state is one of the major factors in promoting the formation of amyloid fibrils by V_L domains.[32,33] We therefore determined the thermodynamic parameters for unfolding of the V_L domains at 37 °C and pH

dx.doi.org/10.1021/bi5007892 | Biochemistry 2014, 53, 5162−5173

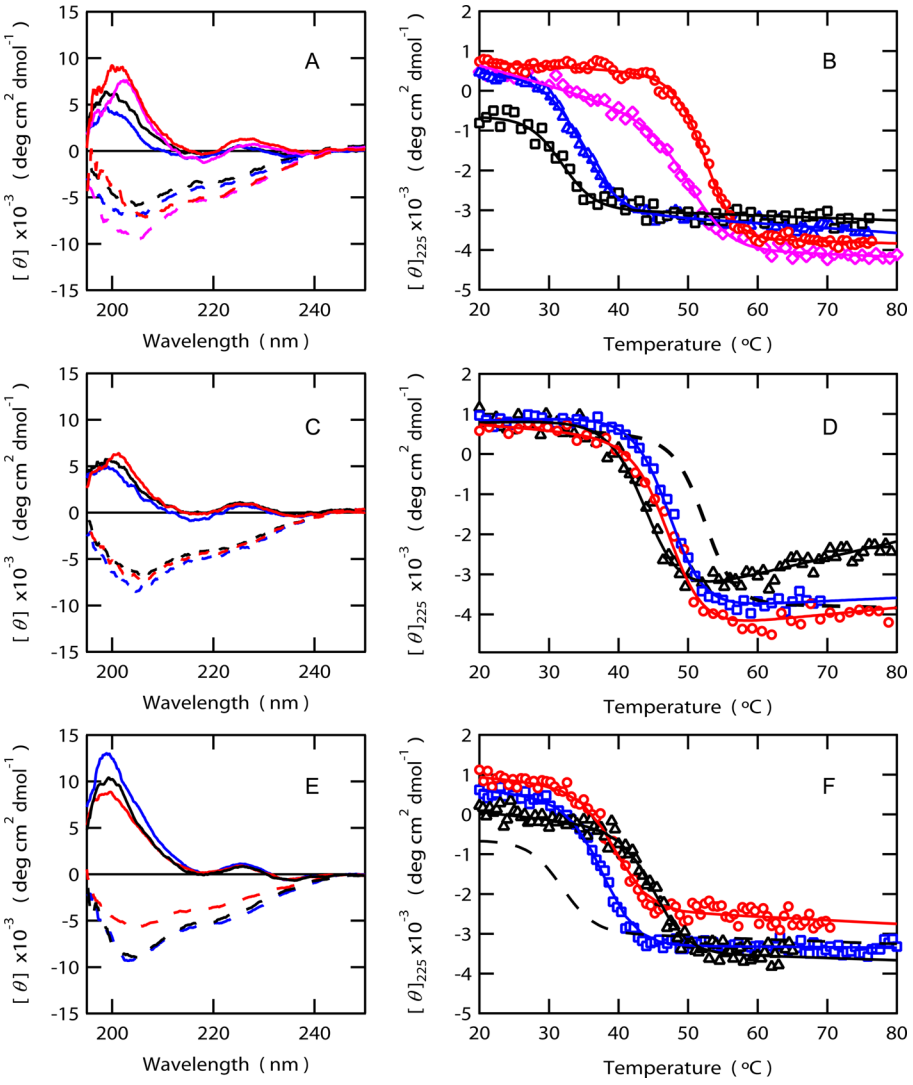

Figure 3. Thermal unfolding transition of the V_Ls as monitored by far-UV CD. (A) Far-UV CD spectra of BRE (black), REI (red), RB45 (blue), and RB51 (magenta) V_L at 20 (—) and 60 °C (– – –) at pH 7.0. (B) Thermal unfolding curves of REI (red circles), BRE (black squares), RB45 (blue triangles), and RB51 (magenta diamonds) V_L monitored by the ellipticity at 225 nm. (C) Far-UV CD spectra of K45N (red), E50D (blue), and K45N/E50D (black) REI V_L at 20 (—) and 60 °C (– – –) at pH 7.0. (D) Thermal unfolding curves of K45N (red circles), E50D (blue squares), and K45N/E50D (black triangles) REI V_L mutants monitored by the ellipticity at 225 nm. The curve fitting result for wild-type REI V_L is also shown (– – –) as a reference. (E) Far-UV CD spectra of N45K (red), D50E (blue), and N45K/D50E (black) BRE V_L at 20 (—) and 60 °C (– – –) at pH 7.0. (F) Thermal unfolding curves of N45K (red circles), D50E (blue squares), and N45K/D50E (black triangles) BRE V_L mutants monitored by the ellipticity at 225 nm. The curve fitting result for wild-type BRE V_L is also shown (– – –) as a reference. The results obtained at different pH values for all the V_L variants are available in Figure S2 of the Supporting Information.

7.0, i.e., under near-physiological conditions where the amyloid fibril formation of wild-type BRE takes place.

Importantly, the data for amyloid formation demonstrated in Figure 2 suggest the possibility of the formation of amyloid fibrils by V_Ls during thermal unfolding experiments. Under thermal conditions where protein molecules aggregate, one cannot obtain reliable thermodynamic parameters for the thermal unfolding reactions. Denaturant-induced unfolding would therefore be an ideal substitute for estimating thermodynamic parameters, particularly for the free energy change upon unfolding (ΔG) at temperatures at which the unfolding study was performed. However, because some amyloidogenic proteins may be unfolded at 37 °C and pH 7.0 in the absence of denaturants, the experiments have to be performed at relatively low temperatures below 37 °C. Under such conditions, reliable thermodynamic parameters for unfolding reactions are difficult to obtain.

In this analysis, we therefore employed thermal unfolding experiments using extremely diluted protein solutions (0.02 mg mL^{-1}) to minimize the probability of forming unfavorable aggregates. Thus, the protein concentration used for the thermal unfolding experiments was 40 times lower than that employed for studies of the aggregation kinetics. We also checked whether the proteins formed irreversible aggregates by comparing the CD spectra of all solutions cooled to 20 °C following the thermal unfolding experiments with spectra obtained at 20 °C prior to these experiments (see Figure S1 of the Supporting Information). All spectra were similar before and after heat-induced unfolding, indicating that the thermal unfolding reactions observed here should be reversible with only small amounts of irreversible aggregates being produced.

dx.doi.org/10.1021/bi5007892 | *Biochemistry* 2014, 53, 5162–5173

Table 1. Thermodynamic Parameters for the Thermal Unfolding Reactions of Chimeric and Point Mutation Variants of REI and BRE V_L at pH 7.0

protein	T_m (°C)	ΔH_m (kJ mol^{-1})	ΔG_U[a] (kJ mol^{-1})	ΔC_p (kJ mol^{-1} K^{-1})
		Wild Type		
REI V_L	52.3 ± 0.1	405.0 ± 4.0	16.0 ± 0.1	8.5 ± 0.4
BRE V_L	31.9 ± 0.1	318.4 ± 2.5	−5.6 ± 0.4	6.4 ± 1.2
		Chimeric Mutants between REI and BRE V_L		
RB45 V_L	34.6 ± 0.2	288.8 ± 2.0	−2.3 ± 0.2	7.4 ± 1.5
RB51 V_L	50.4 ± 0.2	286.5 ± 2.5	10.0 ± 0.3	6.4 ± 1.3
		Point Mutants of REI V_L		
K45N	47.2 ± 0.1	330.5 ± 4.2	9.2 ± 0.1	8.1 ± 0.5
E50D	47.7 ± 0.1	336.0 ± 3.4	9.7 ± 0.1	8.3 ± 0.5
K45N/E50D	43.8 ± 0.1	319.6 ± 1.4	6.3 ± 0.1	8.6 ± 0.1
		Point Mutants of BRE V_L		
N45K	39.4 ± 0.1	323.2 ± 5.7	2.4 ± 0.1	8.7 ± 0.3
D50E	37.6 ± 0.1	317.7 ± 4.2	0.6 ± 0.1	8.1 ± 0.3
N45K/D50E	45.3 ± 0.1	357.4 ± 7.8	8.3 ± 0.3	9.4 ± 0.4

[a]Values at 37 °C calculated according to the Gibbs−Helmholtz equation.

At 20 °C and pH 7.0, V_Ls prepared in this study all exhibited far-UV CD spectra with an intensity minimum at 216 nm, which is suggestive of the presence of β-sheet structures, and a maximum at 225 nm, which is often observed for proteins with an immunoglobulin fold (solid lines in Figure 3A). The peaks at 225 nm probably reflect the presence of aromatic clusters in the native protein structures.[34] These data indicate that all the proteins prepared in this study adopt conformations similar to those of the wild-type proteins at low temperatures. In contrast, at 60 °C, the proteins exhibited spectra typical of the unfolded state with minima around 205 nm.

Figure 3B shows the thermal unfolding curves of the V_L domains at pH 7.0 by monitoring the ellipticity at 225 nm. The data indicated a transition region for REI and RB51 V_L within the temperature range of 45−60 °C, whereas BRE and RB45 V_L showed a transition region within the lower temperature range of 30−40 °C. This result indicates that BRE and RB45 V_L are less stable than RB51 and REI V_L. Importantly, both RB45 and BRE V_L formed amyloid fibrils at 37 °C (Figure 2), while RB51 and REI V_L were resistant to amyloid formation. Thus, these data also support the idea that the V_Ls with more destabilized native states tend to have higher amyloidogenic propensities,[32,33] at least under near-physiological conditions at pH 7.0.

We monitored the unfolding curves of the variant V_Ls at different pH values (see Figure S2 of the Supporting Information) to obtain reliable thermodynamic parameters for unfolding, particularly for the heat capacity change upon unfolding of the proteins (ΔC_p), which is defined as $d\Delta H/dT = d\Delta H_m/dT_m$, where ΔH is the enthalpy change upon unfolding. It is generally difficult to estimate ΔC_p from a single unfolding trace monitored by CD at a single pH, and several unfolding traces with different T_m values at different pH values are required to reliably estimate the ΔC_p value.

As a first approximation, the thermal unfolding curves were analyzed according to the two-state transition between the native and highly unfolded states (see Figure S2 and Table S2 of the Supporting Information). The theoretical curves closely fit the experimental data. The estimated thermodynamic parameters for the unfolding reactions, including the free energy change (ΔG_U) at 37 °C, T_m, ΔH_m, and ΔC_p, are summarized in Table 1.

Importantly, various experimental data indicate that isolated V_L usually assumes a dimeric native structure or is possibly present in a monomer−dimer equilibrium in aqueous solutions.[35−37] However, in this study, we assumed a two-state transition between the monomeric native state and the fully unfolded state. The analysis based on this assumption produced a ΔC_p of 6.4−8.5 kJ mol^{-1} K^{-1} for REI, BRE, RB45, and RB51 V_L (Table 1; see also Table S2 of the Supporting Information). These values are close to that expected for the thermal unfolding reaction of the monomeric native state of any given protein comprising 107 amino acid residues (1.58 ± 0.18 kcal mol^{-1} K^{-1} = 7.61 ± 0.87 kJ mol^{-1} K^{-1}) according to the BPPred server (http://www-clarke.ch.cam.ac.uk/BPPred.php).[38] This result supports the possibility that although the protein assumes the dimeric native state at low temperatures, the major transitions observed here by CD at increased temperatures probably reflect the unfolding reactions of the monomeric native states, the latter initially being produced by dissociation of the dimeric native structures prior to these major transitions taking place at higher temperatures. It is likely that the ellipticity at 225 nm is insensitive to the dissociation of the dimeric native state into the monomeric native state. The possible contribution of the dimeric native state during the thermal unfolding process is examined further in the Discussion.

The results of the analyses described above suggest that the destabilization of the native state under the exact same conditions used for the kinetic experiments of amyloid formation increases the propensity for amyloid fibril formation (Figure 2A,B). According to the thermodynamic parameters in Table 1, we calculated the population of unfolded molecules for each V_L domain at 37 °C and pH 7.0. This analysis clarified that 89.8 and 70.8% of molecules assume the unfolded state in the case of the highly amyloidogenic BRE and RB45 V_L, respectively, whereas the populations of unfolded species for REI and RB51 V_L were much smaller (0.2 and 2.8%, respectively). Thus, the data suggest that the accumulation of the unfolded state should facilitate intermolecular interactions between the unfolded species, thereby promoting the formation of amyloid fibrils. This can be rationalized by the observation that all the V_L domains studied here readily formed amyloid fibrils at 60 °C (Figure 2B), a temperature at which these proteins were almost entirely unfolded (Figure 3B).

dx.doi.org/10.1021/bi5007892 | Biochemistry 2014, 53, 5162−5173

However, even at 60 °C, BRE and RB51 V_L still indicated much higher intensities of thioflavin T fluorescence compared with those of REI and RB45 V_L, as was also the case at 37 °C (Figure 2C). The amounts of unfolded species for both BRE and RB45 V_L at pH 7.0 and 60 °C were calculated to be nearly 100%, while those for REI and RB51 V_L were slightly smaller (97.7 and 96.8%, respectively). Thus, this result suggests that the increased amount of unfolded species present at high temperatures will increase the probability of amyloid fibril formation by facilitating intermolecular interactions between unfolded species. However, a small difference in the amount of unfolded species can affect the rate and final amount of amyloid fibril formation by V_L domains, even under extreme temperature conditions at which the protein molecules are almost entirely unfolded (see the Discussion for further details).

Mutations of Surface-Exposed Residues at Position 45 and/or 50 Affect the Native State Stability and Amyloidogenic Propensity of REI and BRE V_Ls. The results obtained for the chimeric mutants suggested that the population of unfolded species caused by destabilization of the native state increases the probability of amyloid fibril formation by V_Ls. Importantly, the results of the thermal unfolding studies indicated that a difference at only two residue positions between RB51 (K45 and E50) and RB45 (N45 and D50) (Figure 1) significantly alters the native state stability as well as the amyloidogenic propensity. These results suggest that the K45N mutation and/or the E50D mutation of REI V_L probably destabilizes the native state and, as a consequence, increases the amyloidogenic propensity. Conversely, the complementary mutations on BRE V_L (N45K, E50D, and N45K/D50E) should confer stabilization of the native state and decreased amyloidogenicity.

All the mutant proteins indicated the CD spectra are similar to those of the wild type at 20 and 60 °C (Figure 3C,E). As expected, the K45N, E50D, and K45N/E50D mutants of REI V_L all produced destabilized native states with T_m values lower than that of wild-type REI V_L (Figure 3D and Table 1). These mutants also showed increased amyloidogenic propensities at 37 °C based on thioflavin T fluorescence (Figure 2C). The ΔG_U values for K45N (9.2 kJ mol^{-1}) and E50D (9.7 kJ mol^{-1}) at 37 °C and pH 7.0 were decreased compared with the ΔG_U of wild-type REI V_L (16.0 kJ mol^{-1}). The ΔG_U value for the double mutant K45N/E50D was 6.3 kJ mol^{-1}, which is much lower than that for K45N or E50D REI V_L.

In contrast, the N45K, D50E, and N45K/D50E mutants of BRE V_L all produced stabilized native states with T_m values higher than that of wild-type BRE V_L (Figure 3F and Table 1). This result is striking because it is generally difficult to design a mutant protein with a stability higher than that of the wild-type protein, even when using highly sophisticated computational approaches. Moreover, the rate of amyloid formation was decreased by the introduction of these mutations (Figure 2D). N45K/D50E BRE V_L in particular was completely resistant to amyloid formation based on thioflavin T fluorescence, and no change in fluorescence intensity was observed even after incubation for 200 h, as was similarly observed for wild-type REI V_L (Figure 2A). These data for the destabilization and stabilization conferred by the REI and BRE V_L mutants, respectively, indicate that N45 and D50 are key residues for destabilization of the native structure of BRE V_L and the promotion of amyloid fibril formation.

Further analysis of $\Delta\Delta G_U$, $\Delta\Delta H_U$, and $\Delta\Delta S_U$ at 37 °C, which are defined as the differences in ΔG_U, ΔH_U, and ΔS_U, respectively, of the mutant V_L relative to the same values for wild-type V_L (Tables 2 and 3), revealed the thermodynamic mechanisms of stabilization and destabilization of the native states of BRE and REI V_L, respectively, upon introduction of the tested mutations at residues 45 and 50.

Table 2. Values of $\Delta\Delta G_U$, $\Delta\Delta H_U$, $\Delta\Delta S_U$, and $T\Delta\Delta S_U$ of REI V_L Mutants at 37 °C and pH 7.0

mutation	$\Delta\Delta G_U$ (kJ mol^{-1})	$\Delta\Delta H_U$ (kJ mol^{-1})	$\Delta\Delta S_U$ (J mol^{-1} K^{-1})	$T\Delta\Delta S_U$ (kJ mol^{-1})
K45N	−6.8	−26.5	−63.7	−19.8
E50D	−6.2	−28.0	−70.3	−21.8
K45N/E50D	−9.7	−13.6	−12.6	−3.9

Table 3. Values of $\Delta\Delta G_U$, $\Delta\Delta H_U$, $\Delta\Delta S_U$, and $T\Delta\Delta S_U$ of BRE V_L Mutants at 37 °C and pH 7.0

mutation	$\Delta\Delta G_U$ (kJ mol^{-1})	$\Delta\Delta H_U$ (kJ mol^{-1})	$\Delta\Delta S_U$ (J mol^{-1} K^{-1})	$T\Delta\Delta S_U$ (kJ mol^{-1})
N45K	8.0	−48.7	−182.9	−56.7
D50E	6.2	−38.2	−143.2	−44.4
N45K/D50E	13.9	−71.7	−275.9	−85.6

Importantly, for the BRE and REI V_L mutants, both $\Delta\Delta H_U$ and $T\Delta\Delta S_U$ (Tables 2 and 3) produced large, negative values. The decrease observed for ΔH_U may be due to the elimination of specific noncovalent interactions present in the native protein or the change in the extent of hydration of polar and nonpolar groups upon unfolding of the protein molecule.[39] On the other hand, all the mutations produced decreased values of ΔS_U, i.e., negative $\Delta\Delta S_U$, which may be a result of either an increased number of structural fluctuations in the native state or a decreased number of structural fluctuations in the unfolded state. The negative values for both $\Delta\Delta H_U$ and $T\Delta\Delta S_U$ suggest that the native state was entropically stabilized but enthalpically destabilized by these mutations. Taken together, the destabilization of the native states (or negative $\Delta\Delta G_U$) conferred by the REI mutations was enthalpically driven, while the stabilization conferred by the BRE V_L mutations was entropically driven.

DISCUSSION

Our analysis using chimeric mutants of BRE and REI V_L successfully identified the key residues, N45 and D50, responsible for destabilization of the native state of BRE, the causative factor in the higher amyloidogenic propensity of BRE V_L. Although we have clarified the thermodynamic mechanism for the destabilization of the native state by these residues, the structural basis for this phenomenon remains unclear.

In this section, we will discuss the relationship between amyloidogenic propensity and native state stability, particularly for the V_L domains tested in this study, and we will provide a hypothesis about the structural basis of destabilization of the native state based on a comparison of the known crystal structures of REI and BRE V_L.

Relationship between the Rate of Amyloid Formation and ΔG_U. The results obtained in this paper indicate that the destabilization of the native state increases the probability of amyloid fibril formation by V_Ls at pH 7.0. This result is consistent with previous studies using different variants of the V_Ls[8,18−21] and other amyloidogenic proteins.[4,7,26] For these proteins, at least the transient accumulation of partially or fully unfolded species is required prior to the formation of amyloid

dx.doi.org/10.1021/bi5007892 | Biochemistry 2014, 53, 5162−5173

fibrils as the interactions that stabilize the amyloid fibrils differ from those stabilize the native states. It should be noted that although the native state of BRE V_L is highly unstable at pH 7.0, it is more stable than REI V_L at pH 3−5 (Figure S2 and Table S2 of the Supporting Information). Thus, it may be possible that REI V_L indicates an amyloidogenic propensity much higher than that of BRE V_L at acidic pH. Generally, the pH of the physiological environment should be kept at neutral pH, and the decrease in pH may be achieved only under a disease state such as renal tubular acidosis. If the hypothesis about the relationship between native state stability and amyloidogenic propensity is correct, these results suggest that the AL amyloidosis induced by BRE should proceed around pH 7. To simplify the situation, we will consider only the parameters obtained at pH 7.0 in the following discussion.

As already mentioned, V_Ls usually assume a dimeric native state in solution.[35−37] The kinetic analysis of amyloid formation was performed in the presence of 0.8 mg mL^{-1} V_Ls, which is 40 times higher than the concentration used for the thermal unfolding experiments. Thus, the contribution of the dimeric native state may not be negligible particularly under the conditions employed for the kinetic experiments of amyloid formation. We will discuss the reliability of our assumption regarding the two-state transition from a monomeric native state to the unfolded state in the analysis of the thermal unfolding.

According to Chan et al.,[35] the dissociation constant (K_D) of REI V_L at 25 °C and pH 7.5 is 7.5 μM. We also determined the K_D values of REI and BRE V_L based on analytical ultracentrifugation. The K_D values of BRE and REI V_L at 20 °C and pH 7.0 were estimated to be 1.1 ± 0.1 and 2.7 ± 0.2 μM, respectively (S. Unzai and D. Hamada, unpublished data). This result is interesting because REI V_L, with its more stable native state, is more likely to adopt the monomeric native state at pH 7.0 (Figure 3 and Table 1). This suggests that the thermal unfolding transition observed by CD (Figure 3) should reflect the unfolding transitions from the monomeric native state. The fractions of BRE and REI V_L molecules in the monomeric native state were calculated to be 40 and 60%, respectively, at 20 °C and pH 7.0 under the conditions employed in the thermal unfolding studies (Figure 3), where 0.02 mg mL^{-1} V_L was present. We reanalyzed the thermal unfolding curves for BRE and REI V_L at pH 7.0 in Figure 3B on the basis of a three-state mechanism involving dimer dissociation followed by unfolding, assuming that the K_D values for BRE and REI V_L are independent of temperature, i.e., at 2 and 3 μM, respectively. The ΔG_U values of the monomeric native states of BRE and REI V_L were −7.4 and 13.0 kJ mol^{-1} at 37 °C and pH 7.0, respectively. These values are relatively similar to those estimated in the analysis described above (−5.6 and 16.0 kJ mol^{-1}, respectively) obtained by assuming simple two-state transitions from the monomeric native state to the unfolded state (Table 1). If the K_D values for the other V_Ls are also on the order of 1−3 μM, their ΔG_U values (assuming three-state transitions including dimeric and monomeric native states as well as the unfolded state) will be similar to those estimated by assuming a two-state transition from the monomeric native state to the unfolded state (Table 1). Importantly, in the presence of 0.8 mg mL^{-1} protein where the kinetic analyses of amyloid formation by V_L domains (Figure 2) were performed, the fractions comprising the monomeric native state at 20 °C were estimated to be 10 and 14% for BRE and REI V_L, respectively. This suggests that the majority of protein molecules were initially in the dimeric native state during the kinetic analysis of amyloid formation. However, the presence of a low level of the monomeric native state under the same conditions suggests that the unfolding transition proceeds through the native dimer state, then to the native monomer state, and finally to the unfolded state. On the basis of the likely veracity of these assumptions, we suggest that the thermodynamic parameters listed in Table 1 are reliable for inferring the relationship between amyloidogenic propensity and native state stability.

As shown in Figure 4A, the rate constant of amyloid formation [k_{agg} (see Materials and Methods)] obtained from the analysis of the kinetics of amyloid formation was plotted against ΔG_U obtained from the thermal unfolding experiments (see Table 1). This plot represents the tendency for k_{agg} to increase with a decrease in ΔG_U; i.e., the rate of amyloid formation increases with the decreasing stability of the native state. A similar trend was observed when the final fluorescence intensity values for thioflavin T binding (F_{final}) from the aggregation studies were plotted against ΔG_U (Figure 4B).

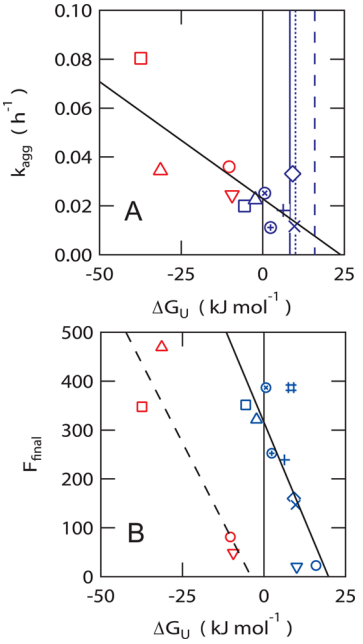

Figure 4. Correlation between amyloidogenic propensity and native state stability of V_Ls. (A) Plot of the rate constant for aggregation (k_{agg}) vs the free energy change upon unfolding (ΔG_U). The solid black line indicates the linear regression result (R^2 = 0.78). (B) Plot of the final intensity of thioflavin T fluorescence observed during the aggregation studies (F_{final}) vs ΔG_U conducted at 37 (blue) and 60 °C (red). The solid and dashed black lines indicate the linear regression result for the data obtained at 37 °C (R^2 = 0.76) and 60 °C (R^2 = 0.91), respectively. The parameters for REI (○), BRE (□), RB45 (△), and RB51 (▽) V_L and K45N (◇), E50D (×), and K45N/E50D (+) REI V_L as well as for N45K (⊕), D50E (⊗), and N45K/D50E (#) BRE V_L were derived from kinetic and thermodynamic analyses of the data shown in Figures 2 and 3, respectively. Because the k_{agg} values for REI, RB51, and N45K/D50E BRE V_L at 37 °C could not be experimentally obtained, their ΔG_U values at 37 °C are represented by the dotted (RB51 V_L), dashed (REI V_L), and solid (N45K/D50E BRE V_L) blue lines.

The plot of k_{agg} versus ΔG_U at 37 °C (Figure 4A, blue symbols) shows no clear correlation between these parameters. However, the correlation becomes apparent when the temper-

dx.doi.org/10.1021/bi5007892 | Biochemistry 2014, 53, 5162−5173

ature is increased to 60 °C (Figure 4A, red symbols). In fact, it is possible to draw a single line by combining the data obtained at 37 and 60 °C with a correlation coefficient (R^2) of 0.78 (Figure 4A, black line). Previous studies of amyloid formation by β-lactoglobulin[26] suggested that k_{agg} correlated with the lag time of amyloid formation. Although the apparently good correlation between k_{agg} and ΔG_U obtained at different temperatures (Figure 4A) can be a coincidence, this result, at least partly, reflects the tendency of the lag time to be shortened by destabilization of the native state.

On the other hand, F_{final} appears to be negatively correlated with ΔG_U at both 37 and 60 °C (Figure 4B, blue and red symbols, respectively); i.e., the final amount of amyloid fibrils formed in solution increases with the decreasing stability of the native state. However, the F_{final} values obtained at 60 °C were correlated with a lower range of ΔG_U values (dashed line) than at 37 °C (solid line). The concentration of free protein remaining in solution after completion of amyloid formation should be equal to the critical concentration for amyloid formation.[40] If F_{final} is proportional to the amount of protein incorporated into amyloid fibrils at the final point of amyloid formation, F_{final} should also negatively correlate with the critical concentration. Thus, the negative correlation between F_{final} and ΔG_U may indicate that ΔG_U is correlated with the critical concentration of amyloid fibril formation.

These results are interesting because the rate of amyloid formation increases at higher temperatures (Figure 4A), although the final amount of protein associated with amyloid fibrils becomes rather diminished (based on the comparison between the F_{final} values along the solid and dashed lines at the same ΔG_U value in Figure 4B). Such behavior may be attributable to the phenomenon of heat-induced dissociation of amyloid fibrils as observed for α-synuclein and β_2-microglobulin as well as fragments thereof.[41] Thus, the increase in the rates of dissociation of the protein from the amyloid fibrils decreases the critical concentration at higher temperatures. As a consequence, the final amount of proteins incorporated into fibrils (F_{final}) decreases at high temperatures despite the increased amount of unfolded molecules following decreases in ΔG_U at such temperatures.

Because REI, RB51, and N45K/D50E BRE V_L did not show any amyloid fibril formation at 37 °C (Figure 2), no k_{agg} values were available for these proteins at this temperature (Figure 4A). The ΔG_U value for REI V_L at 37 °C was the highest among those of the proteins studied here (Table 1). This suggests that the formation of amyloid fibrils by REI V_L was prevented by stabilization of the native state. On the other hand, the ΔG_U values for RB51 and N45K/D50E BRE V_L at 37 °C were similar to that for E50D REI V_L. Nevertheless, only E50D REI V_L showed the formation of amyloid fibrils. This observation indicates that while destabilization of the native state plays a critical role in determining the amyloidogenic propensity of individual V_L domains, this alone is insufficient to fully account for this phenomenon. Additional factors such as differing intrinsic aggregation propensities of different V_L amino acid sequences or differing conformational properties of the various unfolded V_L domains may be responsible for the differences observed in the total amyloidogenic propensity among the various V_L domains.

Structural Basis for the Stabilization and Destabilization of the Native State. Our study revealed the importance of residues 45 and 50 for the stabilization and destabilization of the native states of REI and BRE V_L, respectively. REI V_L mutations K45N and E50D decreased the stability of the native state and facilitated the formation of amyloid fibrils. In contrast, BRE V_L mutations N45K and D50E reduced the amyloidogenic propensity by improving the stability of the native state. The latter result is of significant interest because it is usually challenging to increase the stability of a given protein by mutations at surface-exposed sites. The thermodynamic parameters obtained from the thermal unfolding data suggested that both destabilization and stabilization conferred by these mutations of REI and BRE, respectively, were achieved through decreases in both $\Delta\Delta H_U$ and $T\Delta\Delta S_U$.

Given that no conformational details are yet available for the point or chimeric mutants, it is impossible to elucidate the structural basis of these stability changes in the native states upon introduction of these mutations. However, various probabilities can be predicted from the known native structures and the similarity of the sequences of REI and BRE V_L and other V_Ls. Because the K_D for REI V_L is larger than that for BRE V_L, REI V_L is more likely to be present in the monomeric native state. Nevertheless, ΔG_U for REI V_L is much larger than that for BRE V_L. This indicates that the stabilization of the native state observed in the thermal unfolding studies is unrelated to the difference in free energy between the dimeric and monomeric native states. We will therefore discuss only the properties of the monomeric native structures of REI and BRE V_L.

First, both residues 45 and 50 are solvent-exposed in the native state. Therefore, it is unlikely that mutations of these residues affect the hydrophobic properties of the interior of the native protein. Hence, the tested mutations should modulate only the surface properties of the native state.

Importantly, residue 45 in the V_L domain lies within the FR, in which sequences are well-conserved. According to Déret et al.,[42] as well as the integrated antibody server, abYsis (http://www.bioinf.org.uk/abysis/index.html; see also Figure S3 of the Supporting Information), this site is often occupied by basic residues such as lysine and arginine. The frequencies of arginine and lysine at this position are 56 and 20%, respectively, while the frequency of occurrence of asparagine is only 1%. Nevertheless, the occurrence of asparagine at this site is often found in the V_L domains associated with AL amyloidosis and LCDD.[42] This is consistent with the data obtained for amyloidogenic BRE and nonamyloidogenic REI V_L, which contain N45 and K45, respectively, at this position. Our data for BRE indicate that the substitution of N45 with a lysine may improve the stability of the native state of various amyloidogenic V_L domains and prevent the formation of amyloid fibrils.

According to the native structures of REI (PDB entry 1REI) and BRE V_L (PDB entries 1BRE, 1B0W, and 1QP1), residue 45 is located at the N-terminal end of the βE strands (Figures 1B and 5A,B). The side chains of these residues are exposed to the solvent and form hydrogen bonds with the conserved residue, Q37, in the FR (Figure 5A,B). The hydrogen bond between N45 and Q37 in BRE V_L can be categorized as a bond between two neutral residues, whereas the hydrogen bond between K45 and Q37 in REI V_L is classified as a bond between a charged residue and a neutral residue. It is generally considered that the energy contribution of hydrogen bonds formed between charged and neutral residues is greater than that of hydrogen bonds between neutral residues.[43−45] Thus, the decreased energy contribution of the hydrogen bond between residue 45 and Q37 may be an important factor in the destabilization of

dx.doi.org/10.1021/bi5007892 | Biochemistry 2014, 53, 5162−5173

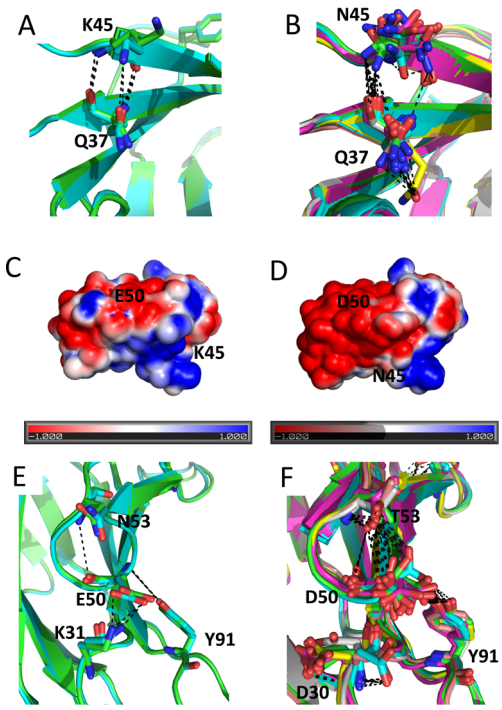

Figure 5. Interactions associated with residues 45 and 50 of REI and BRE V_L. (A) Hydrogen bonds formed between Q37 and K45 in REI V_L. (B) Hydrogen bonds formed between Q37 and N45 in BRE V_L. (C and D) Mapping of the electrostatic potential surface of REI (C) and BRE V_L (D) monomers. Positive to negative electrostatic potentials are colored from blue to red, respectively, as indicated by the scale bar. The electrostatic potentials were calculated by APBS,[46] and the missing hydrogen atoms were built by PDB2PQR[47,48] based on the predicted pK_a of each residue as calculated by PROPKA.[49−52] (E) Salt bridge formed between K31 and E50 in REI V_L. (F) Hydrogen bonds formed among D50, T53, and Y91 in BRE V_L. Monomers in an asymmetric unit present in crystal coordinates of PDB entry 1REI (A and E) or PDB entries 1BRE, 1B0W, and 1QP1 (B and F) are superimposed to show the variations in side chain orientations between monomers in the same crystals.

the native state of K45N REI V_L. On the other hand, in the case of the N45K BRE V_L mutant, the hydrogen bond between the charged (K45) and neutral (Q37) residues may stabilize the native state.

Interestingly, the surface electrostatic potential map of REI V_L confirmed the presence of a positively charged surface localized around K45 (Figure 5C), whereas for BRE V_L, a positive electrostatic potential around N45 is less apparent (Figure 5D). This observation suggests that the K45N REI or N45K BRE V_L mutations also significantly alter the distribution of electrostatic potential on the surface of the native structure, which may possibly affect the thermodynamic stability of the native state.

Unlike for residue 45, residue 50 is contained within the CDR, which is less conserved among the V_Ls (see Figure S3 of the Supporting Information). This site is located at the C-terminal edge of strand βE and is also solvent-exposed in the native structure (Figure 5E,F). Close analysis of the three crystal structures of BRE V_L (PDB entries 1BRE, 1B0W, and 1QP1) suggests that D50 can form a hydrogen bond either with T53 in the loop between strands βE and βF (EF loop) or with Y91 in the loop between strands βH and βI (HI loop). This observation indicates that the side chain of D50 in BRE V_L can form multiple conformers in solution. On the other hand, E50 in REI V_L assumes a salt bridge with K31 that links strands βD and βE. In the case of BRE V_L, position 31 is occupied by the acidic residue, aspartic acid. Thus, D31 in BRE V_L will offer electrostatic repulsion toward D50 in the native state, which may be unfavorable for maintaining the native structure. In this sense, it is unclear why the D50E mutant of BRE V_L increases the native state stability even though the introduction of glutamic acid at this position should also prove to be repulsive toward D31. Possibly, this mutation contributes to the formation of hydrogen bonds involving not only T53 and Y91 but also other residues. Such additional interactions may compensate for the unfavorable interaction between E50 and D31 present in D50E BRE V_L.

According to the crystal structure of REI V_L (PDB entry 1REI), E50 does not form a hydrogen bond with either residue 53 (N53) or 91 (Y91). It is possible that the energy contribution of the salt bridge formed between K31 and E50 is greater than that offered by the hydrogen bonds formed between D50 and T53 or between D50 and Y91 in BRE V_L, because charge−charge attraction is usually stronger than a hydrogen bond. In this sense, the introduction of the additional D31K mutation into D50E or N45K/D50E BRE V_L may further improve the stability of the native state.

Importantly, K31 and E50 in REI V_L are also connected through main chain hydrogen bonds that are required for maintaining the β-sheet structure formed between strands βD and βE. The E50D REI V_L mutation did not alter the type of amino acid present at this position; i.e., it remained an acidic residue. This mutation should therefore not affect the native state stability in an electrostatic manner. However, the E50D REI V_L mutation decreased the length of the alkyl chain in the acidic residue, which may be too short to locate the side chains of K31 and D50 at the proper position for salt bridge formation without distorting the main chain hydrogen bond between K31 in strand βE with the substituted residue of D50 in strand βE. Thus, structural distortion of either the salt bridge or main chain hydrogen bonds between strands βD and βE may have been introduced by the E50D mutation, which we have shown to destabilize the native state of REI V_L.

According to the abYsis server, the frequency of aspartic acid at position 50 (15%) in the case of unstable BRE is relatively higher than the frequency of glutamic acid (8%) found in the more stable REI. This suggests the possibility that the stability of a wild-type κV_L with aspartic acid at this position could be improved via the introduction of the D50E mutation as demonstrated in this study.

In conclusion, our approach in characterizing the stability of chimeric mutants of amyloidogenic BRE and nonamyloidogenic REI V_L successfully identified the key residues, i.e., N45 and D50, critical for destabilization of the native state of BRE V_L. This has been verified not only by the analysis of the destabilized K45N and E50D REI V_L mutants but also by the analysis of the stabilized N45K and D50E BRE V_L mutants. Thus, these results clearly demonstrate not only that destabilization of the native state promotes the formation of amyloid fibrils but also that stabilization of the native state of the V_L domain can actually inhibit this unfavorable reaction. The analysis of the BRE and REI V_L structures implies that the tested mutations modulated the properties of the molecular surface of the native state. Such modulation may also be possible by, e.g., using small molecules that specifically bind to the molecular surface of amyloidogenic V_L domains.

dx.doi.org/10.1021/bi5007892 | *Biochemistry* 2014, 53, 5162−5173

Further analysis of the structural properties of the REI and BRE V_L mutants using X-ray crystallography or NMR should provide additional information about the physicochemical factors in the stabilization and destabilization of these V_L domains.

Finally, a systematic investigation of the critical residues for amyloid formation based on the strategies employed here should provide further insights into the mechanisms of amyloid fibril formation by the various LCs responsible for AL amyloidosis.

■ ASSOCIATED CONTENT

Supporting Information

Experimental details of the recovery yield for refolding following heat-induced unfolding, unfolding curves, a summary of parameters for thermal unfolding obtained at different pH values, and amino acid usage and conservation of residues 45 and 50 in κV_L. This material is available free of charge via the Internet at http://pubs.acs.org.

■ AUTHOR INFORMATION

Corresponding Author

*Telephone: +81 59 231 9611. E-mail: daizo@bio.mie-u.ac.jp.

Author Contributions

Y.K. and H.T. contributed equally to this work.

Funding

This work was supported in part by Grants-in-Aids for the Global COE program A08 (H.H. and D.H.), by a grant for Scientific Research on Innovative Area "Molecular Science of Fluctuations toward Biological Functions" (D.H.), by the Platform for Drug Discovery, Informatics, and Structural Life Science (D.H.) from MEXT, Japan, by a grant for Scientific Research from JSPS (D.H.), and by research grants from The Ichiro Kanehara Foundation for the Promotion of Medical Sciences and Medical Care (D.H.).

Notes

The authors declare no competing financial interest.

■ ACKNOWLEDGMENTS

We thank Drs. T. Tenno, N. Goda, and S. Matsumoto for valuable comments on the manuscript.

■ ABBREVIATIONS

LC, light chain; HC, heavy chain; V_L, variable domain of LC; V_H, variable domain of HC; CDR, complementarity-determining region; FR, framework region; C_{H1}−C_{H3}, constant domains 1−3 of HC, respectively; C_L, constant domain of LC; LCDD, light chain deposition disease; CD, circular dichroism; UV, ultraviolet; PCR, polymerase chain reaction; Tris, tris(hydroxymethyl)aminomethane; EDTA, ethylenediaminetetraacetic acid; PDB, Protein Data Bank.

■ REFERENCES

(1) Dobson, C. M., Šali, A., and Karplus, M. (1998) Protein folding: A perspective from theory and experiment. *Angew. Chem. 110*, 908−935.

(2) Anfinsen, C. B. (1973) Principles that govern the folding of protein chains. *Science 181*, 223−230.

(3) Dobson, C. M. (2003) Protein folding and misfolding. *Nature 426*, 884−890.

(4) Stefani, M. (2004) Protein misfolding and aggregation: New examples in medicine and biology of the dark side of the protein world. *Biochim. Biophys. Acta 1739*, 5−25.

(5) Vendruscolo, M., and Dobson, C. M. (2005) Towards complete descriptions of the free-energy landscape of proteins. *Philos. Trans. R. Soc., A 363*, 433−450.

(6) Bellotti, V., and Chiti, F. (2008) Amyloidogenesis in its biological environment: Challenging a fundamental issue in protein misfolding diseases. *Curr. Opin. Struct. Biol. 18*, 771−779.

(7) Vendruscolo, M., Knowles, T. P., and Dobson, C. M. (2011) Protein solubility and protein homeostasis: A generic view of protein misfolding disorders. *Cold Spring Harbor Perspect. Biol. 3*, a010454.

(8) Pepys, M. B. (2001) Pathogenesis, diagnosis and treatment of systemic amyloidosis. *Philos. Trans. R. Soc., B 356*, 203−210.

(9) Dobson, C. M. (2001) The structural basis of protein folding and its links with human disease. *Philos. Trans. R. Soc., B 356*, 133−145.

(10) Sipe, J. D., Benson, M. D., Buxbaum, J. N., Ikeda, S., Merlini, G., Saraiva, M. J. M., and Westermark, P. (2012) Amyloid fibril protein nomenclature: 2012 recommendations from the nomenclature committee of the international society of amyloidosis. *Amyloid 19*, 167−170.

(11) Hutchinson, A. T., Jones, D. R., and Raison, R. L. (2012) The ability to interact with cell membranes suggests possible biological roles for free light chain. *Immunol. Lett. 142*, 75−77.

(12) Bahlis, N. J., and Lazarus, H. M. (2006) Multiple myeloma-associated AL amyloidosis: Is a distinctive therapeutic approach warranted? *Bone Marrow Transplant. 38*, 7−15.

(13) Rajkumar, S. V., Gertz, M. A., and Kyle, R. A. (1998) Primary systemic amyloidosis with delayed progression to multiple myeloma. *Cancer 82*, 1501−1505.

(14) Gertz, M. A., Lacy, M. Q., and Dispenzieri, A. (1999) Amyloidosis. *Clin. Haematol. 13*, 1211−1233.

(15) Suzuki, K. (2013) Current therapeutic strategy for multiple myeloma. *Jpn. J. Clin. Oncol. 43*, 116−124.

(16) Latif, T., Chauhan, N., Khan, R., Moran, A., and Usmani, S. Z. (2012) Thalidomide and its analogues in the treatment of multiple myeloma. *Exp. Hematol. Oncol. 11*, 27.

(17) Gatt, M. E., and Palladisni, G. (2013) Light chain amyloidosis 2012: A new era. *Br. J. Haematol. 160*, 582−598.

(18) Kim, Y., Wall, J. S., Meyer, J., Murphy, C., Randlph, T. W., Manning, M. C., Solomon, A., and Carpenter, J. F. (2000) Thermodynamic modulation of light chain amyloid fibril formation. *J. Biol. Chem. 275*, 1570−1574.

(19) Stevens, P. W., Raffen, R., Hanson, D. K., Deng, Y.-L., Berrios-Hammond, M., Westholm, F. A., Schiffer, M., Stevens, F. J., Murphy, C., Solomon, A., Eulitz, M., and Wetzel, R. (1995) Recombinant immunoglobulin variable domains generated from synthetic genes provide a system for *in vitro* characterization of light-chain amyloid protein. *Protein Sci. 4*, 421−432.

(20) Wetzel, R. (1997) Domain stability in immunoglobulin light chain deposition disorders. *Adv. Protein Chem. 50*, 183−242.

(21) Blancas-Mejía, L. M., and Ramirez-Alvarado, M. (2013) Systemic amyloidoses. *Annu. Rev. Biochem. 82*, 745−774.

(22) Palm, W. H. (1970) On the isolation, characterisation, and crystallisation of a human Bence-Jones protein of κ type. *FEBS Lett. 10*, 46−48.

(23) Schormann, N., Murrell, J. R., Liepnieks, J. J., and Benson, M. D. (1995) Tertiary structure of an amyloid immunoglobulin light chain protein: A proposed model for amyloid fibril formation. *Proc. Natl. Acad. Sci. U.S.A. 92*, 9490−9494.

(24) Steinrauf, L. K., Chiang, M. Y., and Shiuan, D. (1999) Molecular structure of the amyloid-forming protein κI Bre. *J. Biochem. 125*, 422−429.

(25) Hamaguchi, M., Kamikubo, H., Suzuki, K. N., Hagihara, Y., Yanagihara, I., Sakata, I., Kataoka, M., and Hamada, D. (2013) Structural basis of α-catenin recognition by EspB from enterohaemorrhagic *E. coli* based on hybrid strategy using low-resolution structural and protein dissection. *PLoS One 8*, e71618.

(26) Hamada, D., and Dobson, C. M. (2002) A kinetic study of β-lactoglobulin amyloid fibril formation promoted by urea. *Protein Sci. 11*, 2411−2426.

(27) Epp, O., Lattman, E. E., Schiffer, M., Huber, R., and Palm, W. (1975) The molecular structure of a dimer composed of the variable portions of the Bence-Jones protein REI refined at 2.0-Å resolution. *Biochemistry 14*, 4943−4952.
(28) Naiki, H., Higuchi, K., Matsushima, K., Shimada, A., Chen, W. H., Hosokawa, M., and Takeda, T. (1990) Fluorometric examination of tissue amyloid fibrils in murine senile amyloidosis: Use of the fluorescent indicator, thioflavin T. *Lab. Invest. 62*, 768−773.
(29) Naiki, H., and Nakakuki, K. (1996) First-order kinetic model of Alzheimer's β-amyloid fibril extension *in vitro*. *Lab. Invest. 74*, 374−383.
(30) Ban, T., Hamada, D., Hasegawa, K., Naiki, H., and Goto, Y. (2003) Direct observation of amyloid fibril growth monitored by thioflavin T fluorescence. *J. Biol. Chem. 278*, 16462−16465.
(31) Ban, T., Hoshino, M., Takahashi, S., Hamada, D., Hasegawa, K., Naiki, H., and Goto, Y. (2004) Direct observation of Aβ amyloid fibril growth and inhibition. *J. Mol. Biol. 344*, 757−767.
(32) Hurle, M. R., Helms, L. R., Li, L., Chan, W., and Wetzel, R. (1994) A role for destabilizing amino acid replacements in light-chain amyloidosis. *Proc. Natl. Acad. Sci. U.S.A. 91*, 5446−5450.
(33) Raffen, R., Dieckman, L. J., Szpunar, M., Wunschl, C., Pokkuluri, P. R., Dave, P., Wilkins Stevens, P., Cai, X., Schiffer, M., and Stevens, F. J. (1999) Physicochemical consequences of amino acid variations that contribute to fibril formation by immunoglobulin light chains. *Protein Sci. 8*, 509−517.
(34) Tsybovsky, Y., Shubenok, D. V., Kravchuk, Z. I., and Martsev, S. P. (2007) Folding of an antibody variable domain in two functional conformations *in vitro*: Calorimetric and spectroscopic study of the anti-ferritin antibody V_L domain. *Protein Eng., Des. Sel. 20*, 481−490.
(35) Chan, W., Helms, L. R., Brooks, I., Lee, G., Ngola, S., McNulty, D., Maleeff, B., Hensley, P., and Wetzel, R. (1996) Mutation effects of inclusion body formation in the periplasmic expression of the immunoglobulin V_L domain REI. *Folding Des. 1*, 77−89.
(36) Constantine, K. L., Friedrichs, M. S., Metzler, W. J., Wittekind, M., Hensley, P., and Mueller, L. (1994) Solution structure of an isolated antibody V_L domain. *J. Mol. Biol. 236*, 310−327.
(37) Azuma, T., Kobayashi, O., Goto, Y., and Hamaguchi, K. (1978) Monomer-dimer equilibria of a Bence Jones protein and its variable fragment. *J. Biochem. 83*, 1485−1492.
(38) Geierhaas, C. D., Nickson, A. A., Lindorff-Larsen, K., Clarke, J., and Vendruscolo, M. (2007) BPPred: A computational tool to predict biophysical quantities of proteins. *Protein Sci. 16*, 125−134.
(39) Makhatadze, G. I., and Privalov, P. L. (1990) Heat capacity of proteins. I. Partial molar heat capacity of individual amino acid residues in aqueous solution: Hydration effect. *J. Mol. Biol. 213*, 375−384.
(40) Yagi, H., Hasegawa, K., Yoshimura, Y., and Goto, Y. (2013) Acceleration of the depolymerization of amyloid β fibrils by ultrasonication. *Biochim. Biophys. Acta 1834*, 2480−2485.
(41) Kardos, J., Micsonai, A., Pál-Gábor, H., Petrik, É., Gráf, L., Kovács, J., Lee, Y.-H., Naiki, H., and Goto, Y. (2011) Reversible heat-induced dissociation of β_2-microglobulin amyloid fibrils. *Biochemistry 50*, 3211−3220.
(42) Déret, S., Chomilier, J., Huang, D.-B., Preud'homme, J.-L., Stevens, F. J., and Aucouturier, P. (1997) Molecular modeling of immunoglobulin light chains implicates hydrophobic residues in non-amyloid light chain deposition disease. *Protein Eng. 10*, 1191−1197.
(43) Fersht, A. R., Shi, J. P., Knill-Jones, J., Lowe, D. M., Wilkinson, A. J., Blow, D. M., Brick, P., Carter, P., Waye, M. M., and Winter, G. (1985) Hydrogen binding and biological specificity analysed by protein engineering. *Nature 314*, 235−238.
(44) Burley, S. K., and Petsko, G. A. (1988) Weakly polar interactions in proteins. *Adv. Protein Chem. 39*, 125−189.
(45) Ippolito, J. A., Alexander, R. S., and Christianson, D. W. (1990) Hydrogen bond stereochemistry in protein structure and function. *J. Mol. Biol. 215*, 457−471.
(46) Baker, N. A., Sept, D., Joseph, S., Holst, M. J., and McCammon, J. A. (2001) Electrostatics of nanosystems: Application to microtubules and the ribosome. *Proc. Natl. Acad. Sci. U.S.A. 98*, 10037−10041.
(47) Dolinsky, T. J., Czodrowski, P., Li, H., Nielsen, J. E., Jensen, J. H., Klebe, G., and Baker, N. A. (2007) PDB2PQR: Expanding and upgrading automated preparation of biomolecular structures for molecular simulations. *Nucleic Acids Res. 35*, W522−W525.
(48) Dolinsky, T. J., Nielsen, J. E., McCammon, J. A., and Baker, N. A. (2004) PDB2PQR: An automated pipeline for the setup, execution, and analysis of Poisson-Boltzmann electrostatics calculations. *Nucleic Acids Res. 32*, W665−W667.
(49) Søndergaard, C. R., Olsson, M. H. M., Rostkowski, M., and Jensen, J. H. (2011) Improved treatment of ligands and coupling effects in empirical calculation and rationalization of pK_a values. *J. Chem. Theory Comput. 7*, 2284−2295.
(50) Olsson, M. H. M., Søndergaard, C. R., Rostkowski, M., and Jensen, J. H. (2011) PROPKA3: Consistent treatment of internal and surface residues in empirical pK_a predictions. *J. Chem. Theory Comput. 7*, 525−537.
(51) Bas, D. C., Rogers, D. M., and Jensen, J. H. (2008) Very fast prediction and rationalization of pK_a values for protein-ligand complexes. *Proteins 73*, 765−783.
(52) Li, H., Robertson, A. D., and Jensen, J. H. (2005) Very fast empirical prediction and interpretation of protein pK_a values. *Proteins 61*, 704−721.